Chemical and dynamical discontinuity at the extratropical tropopause based on START08 and WACCM analyses

A. Kunz,[1,2] L. L. Pan,[2] P. Konopka,[1] D. E. Kinnison,[2] and S. Tilmes[2]

Received 5 August 2011; revised 2 October 2011; accepted 19 October 2011; published 17 December 2011.

[1] Using isentropic trace gas gradients of O_3 and CO, the discontinuity in the chemical composition of the upper troposphere (UT) and lower stratosphere (LS) is examined on middle world isentropes from 300 to 380 K. The analysis is a follow-up study of the dynamical discontinuity as represented by the potential vorticity (PV) gradient-based tropopause, which is based on the product of isentropic PV gradients and wind speed. Overall, there is fairly good consistency between the chemical discontinuity in trace gas distributions and the PV gradient-based tropopause. Trace gas gradients at the PV gradient-based tropopause are stronger in winter than in summer, revealing the seasonal cycle of the tropopause transport barrier. The analysis of the trace gas gradients also identifies atmospheric transport pathways in the upper troposphere–lower stratosphere (UTLS). Several regions where trace gas gradients are found to be decoupled from the dynamical field indicate preferred transport pathways between the UT and LS. In particular, anomalous CO and O_3 gradients above eastern Africa, eastern Asia, and the West Pacific are likely related to convective transport, and anomalous O_3 gradients over the North Atlantic and North Pacific are related to isentropic transport connected to frequent wave breaking. The results indicate that the PV gradient-based tropopause definition provides a good identification of the dynamical and chemical discontinuity and is therefore effective in locating the physical boundary in the UTLS.

Citation: Kunz, A., L. L. Pan, P. Konopka, D. E. Kinnison, and S. Tilmes (2011), Chemical and dynamical discontinuity at the extratropical tropopause based on START08 and WACCM analyses, *J. Geophys. Res.*, *116*, D24302, doi:10.1029/2011JD016686
.

1. Introduction

[2] The tropopause separates the well-mixed troposphere from the stratified stratosphere and often behaves like a quasi-material surface [*Holton et al.*, 1995]. This quasi-material surface reflects a barrier of air mass exchange between the upper troposphere (UT) and lower stratosphere (LS) [*Haynes and Shuckburgh*, 2000; *Haynes et al.*, 2001]. The UTLS is a region of strong coupling among dynamics, chemistry and radiation. Cross-tropopause exchange processes affect the distribution of climate-relevant trace gases and the radiative balance at the tropopause. In addition, a change in the atmospheric trace gas composition in the UTLS, in particular O_3 or H_2O, has the potential to affect the surface climate [*Forster and Shine*, 1997; *Solomon et al.*, 2010]. An accurate definition of the tropopause that captures the physical and chemical changes from the troposphere to the stratosphere is therefore an important element for quantifying the role of the UTLS in chemistry-climate coupling.

[3] Stratosphere-troposphere exchange (STE) is known to be well related to the UTLS dynamical flow structure and meteorological processes [*Stohl et al.*, 2003]. Jet streams [*Cadle et al.*, 1969; *Ray et al.*, 2004], tropopause folds [*Cadle et al.*, 1969; *Danielsen and Mohnen*, 1977; *Shapiro*, 1980; *Shapiro et al.*, 1987], and tropospheric intrusions associated with double tropopauses [*Pan et al.*, 2009; *Homeyer et al.*, 2011] affect the distribution and variability of trace gas constituents across the tropopause. The dynamically induced trace gas variability in the UTLS is highlighted by the significant correlation between O_3 and potential vorticity (PV) [*Danielsen*, 1968]. The concept of the dynamical tropopause is therefore largely motivated by the need to quantify STE processes.

[4] In contrast to the thermal tropopause, which is identified with the help of the vertical temperature lapse rate [*World Meteorological Organization*, 1957], the dynamical tropopause was first introduced as a discontinuity in the isentropic PV field [*Reed*, 1955]. Subsequently, it is often defined by a selected PV isosurface that separates air masses with high PV in the stratosphere from air masses with low PV in the troposphere, and is characterized by a band of enhanced gradients of PV [*Hoskins et al.*, 1985; *Holton et al.*, 1995; *Schwierz et al.*, 2004; *Martius et al.*, 2010]. The strong isentropic PV gradients at the tropopause are maintained by dynamical effects of synoptic scale baroclinic eddies in the UT [*Held*, 1982] and are a result of a partial dynamic barrier to transport of air masses in the UTLS [*Haynes and Shuckburgh*, 2000; *Haynes et al.*, 2001]. This barrier is

[1]Institut für Energie- und Klimaforschung: Stratosphäre, Forschungszentrum Jülich, Jülich, Germany.
[2]National Center for Atmospheric Research, Boulder, Colorado, USA.

Copyright 2011 by the American Geophysical Union.
0148-0227/11/2011JD016686

noticeable as an abrupt change in trace gases [*Danielsen and Hipskind*, 1980]. So far, it is conventional to define the dynamical tropopause by ad hoc chosen PV values [e.g., *World Meteorological Organization*, 1986; *Hoerling et al.*, 1991; *Holton et al.*, 1995], e.g., the 2 PVU isosurface following [*Holton et al.*, 1995]. Nevertheless, it is unclear which PV value is optimal to represent the chemical transition from the troposphere to the stratosphere.

[5] The conceptual definition of the dynamical tropopause by *Reed* [1955] has recently been implemented in an algorithm [*Kunz et al.*, 2011]. This algorithm is similar to the method of determining the edge of the polar vortex [*Nash et al.*, 1996], and defines the location of the highest potential vorticity gradient, constrained by the wind speed, on an isentrope as the dynamical tropopause. In particular, this PV gradient–based dynamical tropopause is determined as maximum of the product of the PV gradient and the horizontal wind speed with equivalent latitudes on isentropes. The location of this tropopause is therefore represented by an equivalent latitude, φ_e^{TP}, or the associated PV isoline, PV^{TP}, and describes a quasi–material surface through PV isolines varying from isentrope to isentrope and with season. *Kunz et al.* [2011] showed that PV^{TP} represents the dynamical discontinuity and it follows the maximum horizontal wind speed on all middle world isentropes in accordance with the maximum isentropic PV gradients occurring in the vicinity of the jet streams near the tropopause [*Martius et al.*, 2010]. Since the PV value that represents the maximum gradient varies between isentropes and with season, it overcomes the limitation of using a particular PV isosurface for all isentropes.

[6] This work examines, as a follow-up study, how well the PV gradient-based tropopause represents the transition in the trace gas fields between the UT and LS. An isentrope-based analysis of the location of the chemical discontinuity in comparison to the location of the PV gradient-based tropopause, i.e., the dynamical discontinuity, is presented. A detailed study of the exact locations on isentropes where the chemical and dynamical discontinuities agree with each other as well as where they disagree allows answering the following questions: (1) Is there consistency between the chemical (O_3 and CO) and dynamical discontinuity (PV) in the UTLS? (2) Do isentropic trace gas gradients reveal preferred transport pathways in the UTLS?

[7] To address these questions, the isentropic distribution of trace gas fields relative to the PV gradient-based tropopause is analyzed. Two trace gases with opposite dominant source regions in the atmosphere are used in this paper: O_3 as a tracer with dominant sources in the stratosphere, and CO as a tracer with dominant sources in the troposphere. These trace gases have been widely used as transport tracers because their lifetimes in the UTLS are ideal to reflect the influence of dynamical processes in this region [*Folkins et al.*, 2006].

[8] To study the chemical discontinuity in the tropopause region, both in situ measured O_3 and CO of the START08 (Stratosphere-Troposphere Analyses of Regional Transport 2008) campaign and simulated fields based on WACCM (Whole Atmosphere Community Climate Model) are used. These O_3 and CO data are isentropically analyzed using a new coordinate, the relative equivalent latitude of the measurement location with respect to PV^{TP}. This is a complimentary approach to the investigation of the chemical discontinuity at the tropopause at altitude levels relative to the thermal tropopause [e.g., *Pan et al.*, 2004; *Hegglin et al.*, 2009; *Tilmes et al.*, 2010; *Manney et al.*, 2011].

[9] This paper is structured as follows. Section 2 contains a description of the data sets used. The isentropic distribution of trace gas data observed during START08 is presented in section 3. Section 4 compares WACCM isentropic gradients of trace gases with the PV gradient-based tropopause. The PV gradient-based tropopause as a transport barrier is also discussed in this section. Both the relevance and the limitation of the PV gradient-based approach to represent the dynamical and chemical discontinuity are discussed in section 5.

2. Data Description

2.1. START08 Data

[10] The Stratosphere-Troposphere Analyses of Regional Transport 2008 (START08) experiment [*Pan et al.*, 2010] was conducted using the new National Science Foundation (NSF)–National Center for Atmospheric Research (NCAR) Gulfstream V (GV) research aircraft. The experiment was designed to establish a better connection between the chemical structure of the UTLS and atmospheric dynamics. Eighteen research flights were performed, with five flights in April, seven flights in May and six flights in June. These flights encompass at least 123 flight hours up to a ceiling altitude of 14.3 km, and span a range of isentropes roughly between 280 and 400 K. A number of meteorological scenarios in the extratropical UTLS were observed above central North America (25°N–65°N, 80°W–120°W). Tropospheric intrusions into the stratosphere associated with double tropopause events or stratospheric intrusions into the troposphere by tropopause folds [*Vogel et al.*, 2011; *Homeyer et al.*, 2011], gravity wave generation and convective transport were probed. A large range of trace gas measurements were made during START08 and this work uses O_3 and CO trace gas data to study the chemical discontinuity at the tropopause. The O_3 and CO data are provided at 1 s interval (1 Hz sampling rate). These samples represent approximately 200 m horizontal resolution.

2.2. SD-WACCM Data

[11] The Whole Atmosphere Community Climate Model, Version 4 (WACCM4) is a fully interactive chemistry climate model, where the radiatively active gases affect heating and cooling rates and therefore dynamics [*Garcia et al.*, 2007]. The vertical domain extends from the surface to the lower thermosphere. The vertical resolution is variable: ≈3.5 km above 65 km, ≈1.75 km around the stratopause (50 km), 1.1–1.4 km in the lower stratosphere (below 30 km), and ≈1.1 km in the troposphere (except near the ground where much higher vertical resolution is used in the planetary boundary layer). The horizontal resolution used for this work is 1.9° × 2.5° in latitude and longitude.

[12] Recently, a new version of the WACCM4 model has been developed that allows the model to be run with specified (external) meteorological fields [*Lamarque et al.*, 2011]. These meteorological fields, M_{geos}, come from the NASA Global Modeling and Assimilation Office (GMAO) Goddard Earth Observing System Model, Version 5 (GEOS-5). Here,

temperature, zonal and meridional winds, and surface pressure are used to drive the physical parameterization that control boundary layer exchanges, advective and convective transport, and the hydrological cycle. In this study, a "nudging" approach is used where the simulated meteorological fields, M_{sim}, are calculated in the following manner:

$$M_{sim} = M_{geos} \cdot \alpha + (1 - \alpha) \cdot M_{int}. \quad (1)$$

[13] M_{int} and M_{geos} are the meteorological fields from the interactive model and GEOS-5, respectively. The fraction α of M_{geos} used in this study is 0.01 (i.e., 1% of the M_{sim} fields are from GEOS-5). This "nudging" approach is applied at every model time step (i.e., every 30 min). For the meteorological fields this nudging scheme is applied from the surface to 50 km; above 60 km the model meteorological fields are fully interactive, with a linear transition in between. The vertical transport is derived from the divergence of the M_{sim} horizontal winds. Even with a small fraction of the GEOS-5 meteorological used at every time step, the resulting M_{sim} fields accurately represent the original GEOS-5 meteorological fields.

[14] The chemical module of WACCM4 is based upon the three-dimensional chemical transport Model for OZone And Related chemical Tracers, Version 4 [*Kinnison et al.*, 2007]. WACCM4 includes a detailed representation of the chemical and physical processes in the troposphere through the lower thermosphere. The species included within this mechanism are contained within the O_x, NO_x, HO_x, ClO_x, and BrO_x chemical families, along with CH_4 and its degradation products. In addition, fourteen primary nonmethane hydrocarbons and related oxygenated organic compounds are included [*Emmons et al.*, 2010]. This "base" mechanism contains 122 species, more than 220 gas-phase reactions, 71 photolytic processes, and 18 heterogeneous reactions on multiple aerosol types.

[15] The SD-WACCM4 simulation employed here corresponds to the time period from 1 January 2004 through the end of 2008. For this simulation the model had a spin-up time from 1980 to the end of 2003 in fully interactive mode, i.e., WACCM without specified dynamics. On 1 January 2004 the model was switched to SD-WACCM4 with the nudging approach as described earlier.

[16] Here, we interpolate the output of the multiyear SD-WACCM4 run from 2004 to 2008 on middle world isentropes between 300 and 380 K with a 5 K discretization. The PV values on each isentrope are transformed into equivalent latitudes varying between −90°S and 90°N according to *Butchart and Remsberg* [1986] to calculate the PV gradient-based tropopause [*Kunz et al.*, 2011].

2.3. ECMWF Data

[17] Potential vorticity is also calculated from the T511L60 operational ECMWF analysis fields [*Simmons et al.*, 2005] for the 18 START08 research flight days in 2008. The data are interpolated on a 1° × 1° horizontal grid and to 35 vertical pressure levels (19 equidistant levels between 1000 and 100 hPa). The vertical resolution is ~0.8–1.4 km around the extratropical tropopause. These ECMWF data on pressure levels are then interpolated on isentropic θ levels. This is again done for middle world isentropes between 300 and 380 K with a discretization of 5 K.

3. START08 Isentropic Distribution of O_3 and CO

[18] Observations during the START08 experiment focus on the extratropical UTLS with a high frequency of measurements on isentropes between 300 and 380 K in the vicinity of the tropopause and jet streams. Figures 1a–1c show the counts of START08 O_3 and CO data points in equivalent latitude, φ_e, and theta, θ, coordinates separately for April, May and June. The counts represent the number of 1 s samples in each 5° equivalent latitude and 5 K potential temperature bin. Also shown is the equivalent latitude of the gradient based tropopause, φ_e^{TP}, the zonal wind speed and the 2 PVU isosurface calculated using ECMWF operational fields for each START08 flight day. The zonal mean of the zonal wind speed and PV are calculated in the longitude range λ = 80°W–120°W which were covered by the START08 flights. The location of the PV gradient-based tropopause in Figure 1 is determined by calculating φ_e^{TP} on ECMWF isentropes and averaging these over all START08 flight days.

[19] The φ_e-θ presentation of START08 data shows observations both poleward and equatorward of φ_e^{TP}. The data density is highest in the vicinity of the extratropical thermal and PV gradient-based tropopauses. The poleward movement of φ_e^{TP} from April to May is associated with the seasonal behavior of the jet streams. Both the subtropical jet stream with a mean jet core at 350 K and the polar jet stream with its mean jet core at 320 K are related to φ_e^{TP}. The maximum of the wind field on isentropes above the subtropical jet core at 350 K is better represented by φ_e^{TP} than by the 2 PVU isosurface. On these isentropes the 2 PVU isoline moves toward the equator and does not follow the maximum wind speed pattern.

[20] Figures 1d–1f show the mean isentropic distribution of O_3 in φ_e-θ coordinates. The background value of O_3 is lower than 100 ppbv in the troposphere and higher than 300 ppbv in the stratosphere. The transitional value of O_3 from the troposphere to the stratosphere, indicated by a strong isentropic gradient, is roughly between 100 and 300 ppbv. The range of φ_e covering this transitional region varies with isentrope, e.g., in April it spans a larger meridional region on isentropes below the subtropical jet stream than on isentropes above. These observed background values of O_3 during START08 are consistent with UTLS O_3 climatologies for spring and summer based on ozonesonde and aircraft data [*Logan*, 1999; *Tilmes et al.*, 2010]. The PV gradient-based tropopause, φ_e^{TP}, and the thermal tropopause, TP_{th}, are associated with O_3 mixing ratios of 100–300 ppbv dependent on isentrope. The variation of φ_e^{TP} with isentrope is followed by a band of strong O_3 gradients. In the seasonal mean, φ_e^{TP} identifies the isentropic transition of O_3 from the troposphere to the stratosphere better than the 2 PVU isosurface.

[21] The mean isentropic distribution of CO is shown in Figures 1g–1i. The background value of the tropospheric tracer CO is higher than 80 ppbv in the troposphere and lower than 40 ppbv in the stratosphere. There is a sharp transition in CO mixing ratios from 40 to 80 ppbv across the

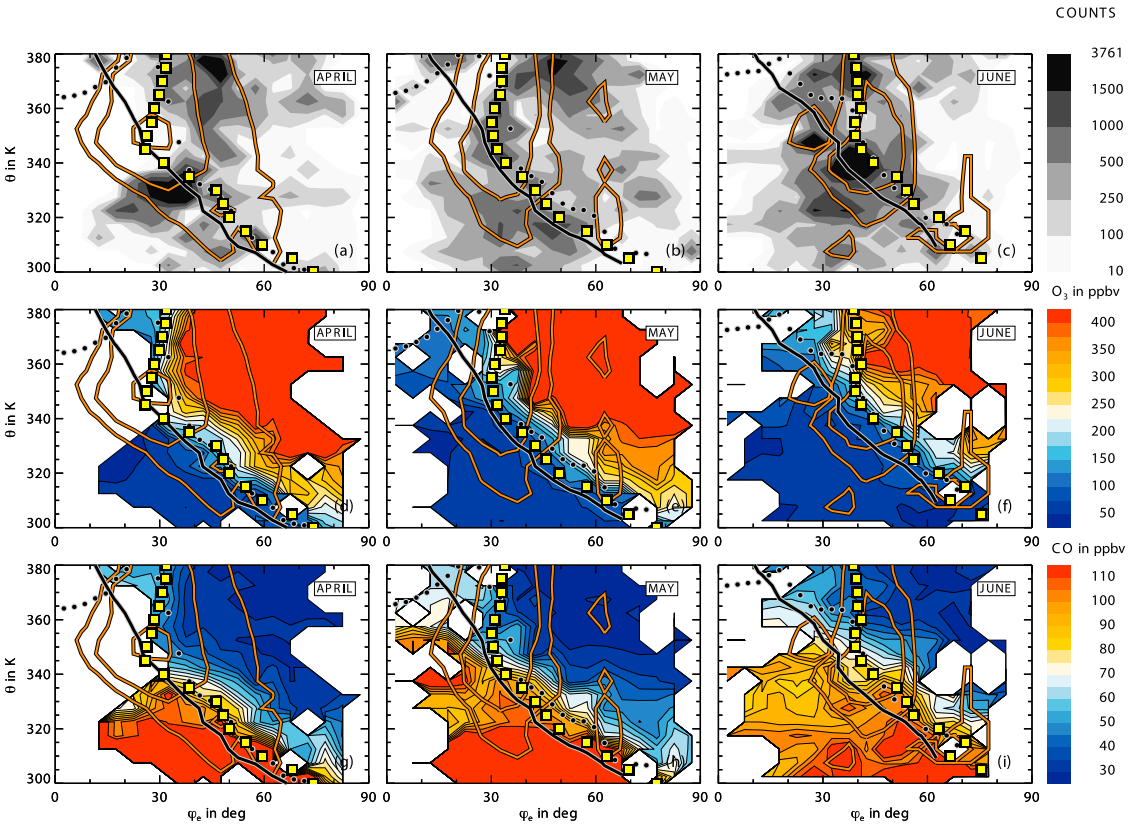

Figure 1. (a–c) Monthly counts of data, (d–f) mean O_3, and (g–i) mean CO with equivalent latitude observed during START08 from April to June. The means are representative for 5° equivalent latitude and 5 K potential temperature bins. PV^{TP} is highlighted by yellow squares. The zonal means of zonal wind speed (orange contours) of the 2 PVU isoline (black contour) and of the thermal tropopause (black dots) are calculated from ECMWF fields within the longitude range covering START08 flights.

PV gradient-based tropopause from spring to summer. This mixing ratio range is consistent with the aircraft data–based climatology of *Tilmes et al.* [2010]. The transitional isentropic distribution of CO connected to an enhanced isentropic gradient also follows φ_e^{TP}, especially on isentropes below the subtropical jet core (350 K). In contrast to O_3, the relationship between the CO gradient and φ_e^{TP} is weaker above 350 K, as shown by this START08 data sampling. The advantage of φ_e^{TP} to represent the transition of CO in the UTLS is not as obvious as for O_3.

[22] In Figure 2, the relative equivalent latitude coordinate, $\Delta\varphi_e^{TP}$, is introduced. $\Delta\varphi_e^{TP}$ is the isentropic equivalent latitude difference between the measurement location, φ_e^m, and φ_e^{TP}, i.e.,

$$\Delta\varphi_e^{TP} = \varphi_e^m - \varphi_e^{TP}. \quad (2)$$

[23] Negative $\Delta\varphi_e^{TP}$ values indicate measurements in the troposphere or equatorward of φ_e^{TP} and positive $\Delta\varphi_e^{TP}$ values indicate measurements in the stratosphere or poleward of φ_e^{TP}.

[24] Figures 2a and 2d show the isentropic O_3 and CO distribution in relative equivalent latitudes for all isentropes between 300 and 380 K in May. The counts of O_3 and CO data are calculated in 5° $\Delta\varphi_e^{TP}$ bins and 20 ppbv O_3 or 10 ppbv CO bins, respectively. The mean profiles of O_3 and CO averaged over 300–380 K relative to φ_e^{TP}, i.e., in $\Delta\varphi_e^{TP}$ bins, show a sharp transition across the tropopause ($\Delta\varphi_e^{TP} = 0$) from the upper troposphere ($\Delta\varphi_e^{TP} < 0$) to the lower stratosphere ($\Delta\varphi_e^{TP} > 0$). The relative equivalent latitude difference between the 2 PVU isoline and the measurement position, $\Delta\varphi_e^{2PVU}$, shows a less sharp trace gas transition across the tropopause. There is an offset of the mean profiles of O_3 and CO relative to 2 PVU toward positive $\Delta\varphi_e^{2PVU}$ in the stratosphere. This offset is obvious on high isentropes, e.g., 370 K (Figures 2c and 2f), rather than on low isentropes, e.g., 330 K (Figures 2b and 2e). As shown by *Kunz et al.* [2011] the PV values representative for φ_e^{TP} increase with potential temperature. At 370 K they are much higher than 2 PVU due to higher gradients in potential temperature around this isentrope, whereas the 2 PVU approximately represents the tropopause in spring at 330 K. This behavior results in an increased offset of mean trace gas distributions in $\Delta\varphi_e^{2PVU}$ coordinates on higher isentropes toward the stratospheric side on higher isentropes.

[25] These results show that the PV gradient-based tropopause marks the troposphere to stratosphere transition of isentropic O_3 and CO distributions in the high-resolution aircraft data. However, these aircraft data are limited in their spatial and temporal coverage. In order to investigate the seasonal and spatial variability of the trace gas gradients in

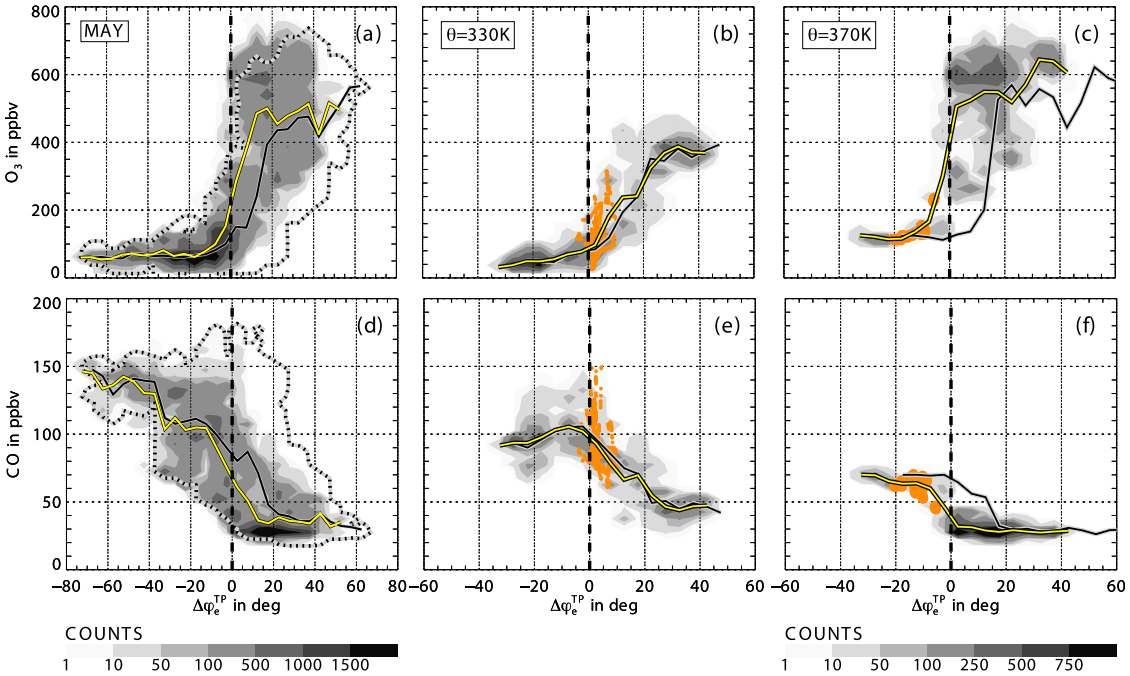

Figure 2. (a and d) Counts of START08 O_3 and CO data relative to PV^{TP} in equivalent latitude distance, $\Delta\varphi_e^{TP}$, during May between 300 and 380 K isentropes and for two different isentropes: (b and e) 330 and (c and f) 370 K (gray shaded contours). Positive $\Delta\varphi_e^{TP}$ represents data poleward of PV^{TP} in the stratosphere, and negative $\Delta\varphi_e^{TP}$ represents data in the troposphere equatorward of PV^{TP}. The distribution of data relative to the 2 PVU isoline in $\Delta\varphi_e^{2PVU}$ distance is surrounded by the black-gray dashed contour representing the count 1. Mean profiles of O_3 and CO relative to PV^{TP} (yellow line) and relative to 2 PVU (black line) are shown. The PV range between 2–4 PVU in $\Delta\varphi_e^{TP}$ is highlighted in orange.

the UTLS, WACCM data are examined for the entire Northern Hemisphere.

4. WACCM Isentropic Gradient of O_3 and CO

[26] The absolute values of meridional O_3 and CO gradients are analyzed on middle world isentropes between 300 and 380 K for the Northern Hemisphere. The absolute gradient of the trace gas mixing ratio μ is calculated with latitude φ as follows:

$$\nabla\mu = |\mathrm{grad}(\ln\mu)| = \left|\frac{\partial \ln\mu}{\partial\varphi}\right| = \left|\frac{1}{\mu}\frac{\partial\mu}{\partial\varphi}\right|. \quad (3)$$

[27] To emphasize the sharp transition of O_3 and CO across the tropopause (Figures 1 and 2) the respective isentropic gradients, i.e., ∇O_3 and ∇CO, are calculated for logarithmic mixing ratios. These gradients are therefore dependent on the dimension of φ. The gradients are calculated daily from 2004 to 2008.

[28] Compared to the standard approach, the calculation of the gradient for logarithmic trace gas mixing ratios means that the gradient in mixing ratio is scaled by a factor dependent on the inverse mixing ratio, i.e., $1/\mu$ (equation (3)). This factor scales down the gradients of the trace gases with strongest weighting in their respective dominant source regions. In particular, the values of ∇O_3 are smaller in the stratosphere poleward of PV^{TP} compared to a standard approach without using the logarithm of the mixing ratio. This discrepancy is strongest on isentropes higher than 350 K during spring, when the stratosphere is influenced by the large-scale downward transport of air masses containing high O_3 due to the residual circulation. The values of ∇CO are scaled down in the troposphere equatorward of PV^{TP} in regions of strong convection influenced by an upward transport of high CO from the boundary layer. *Hegglin et al.* [2010] used a similar motivated approach and normalized their CO gradients in tropopause coordinates with respect to their mean tropospheric values to separate influences of the troposphere.

[29] This study focuses on the analysis of the tropopause region and therefore makes use of the logarithm for identifying strong trace gas gradients at the tropopause and separating them from processes outside the UTLS which are not relevant here. It should be also noted that the inverse trace gas factor shifts the gradients toward smaller trace gas values by definition, i.e., compared to a standard approach of the gradient without using the logarithm of the trace gases the maximum isentropic gradient of CO (O_3) is slightly shifted toward the LS (UT) (see also section 4.1).

4.1. Example Isentropic Trace Gas Fields and Gradients

[30] Figures 3a and 3b show a selected cross section of O_3 and CO, respectively, and of the corresponding isentropic trace gas gradients (Figures 3c and 3d) in φ-θ coordinates at $\lambda = 140°$ on 25 February 2008. Maximum ∇O_3 and ∇CO are shown to be in the vicinity of the PV gradient-

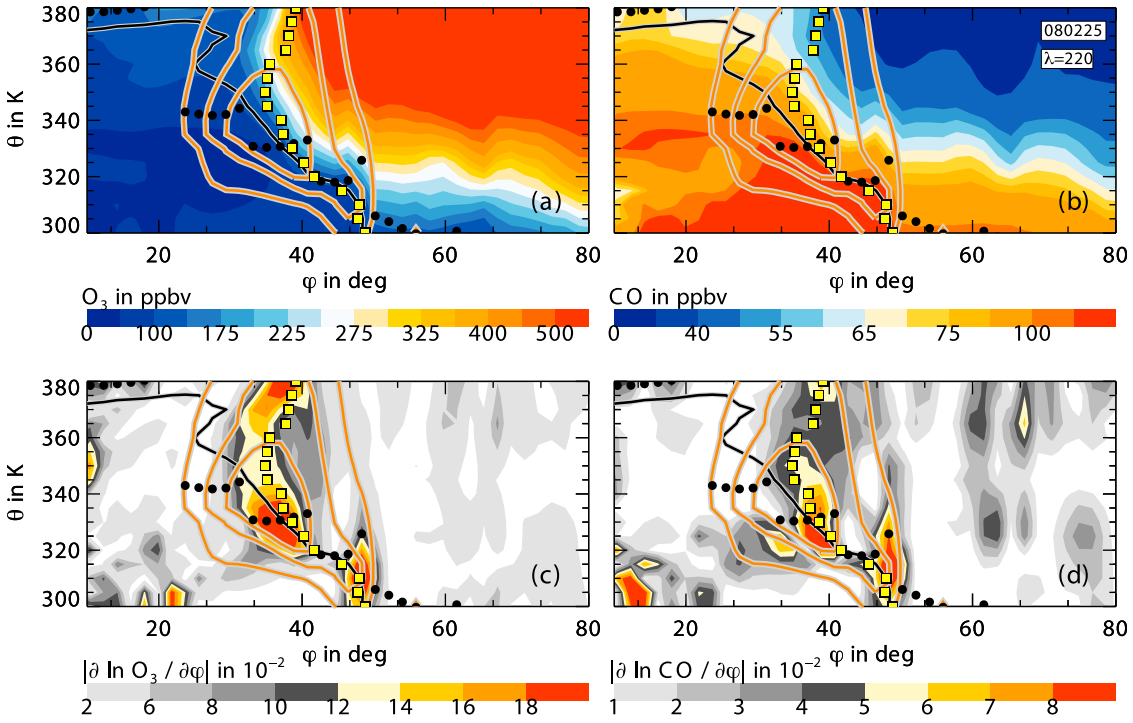

Figure 3. Instantaneous WACCM isentropic distribution of (a and b) O_3 and CO and (c and d) their gradients on 25 February 2008 at the 220° longitude. PV^{TP} (yellow squares), 2 PVU isoline (black line), and horizontal wind speed (orange contours) are shown. The thermal tropopause is indicated by black dots.

based tropopause, PV^{TP}, and the wind maxima on each isentrope.

[31] The influence of the inverse trace gas factor $1/\mu$ is particularly obvious in the maximum of the isentropic gradient of O_3. Especially on isentropes higher than 320 K in regions of a strong isentropic gradient of O_3 the maximum ∇O_3 is shifted slightly toward the UT compared to PV^{TP}. By using a standard approach there would be an improved agreement between PV^{TP} and the trace gas gradient. ∇CO does not show this shift as strong as ∇O_3.

[32] In particular, pronounced ∇O_3 and ∇CO maxima are seen on distinct isentropes (310, 330, and 380 K) in the vicinity of PV^{TP} and the wind speed maxima. The chemical and the dynamical discontinuity are related in this case study. The seasonal mean relationship between the chemical and the dynamical discontinuity is investigated in section 4.2.

4.2. Seasonal Mean Isentropic Gradients With Equivalent Latitude

[33] The daily isentropic gradients of O_3 and CO in φ-θ coordinates are sampled for different seasons, i.e., data arrays are generated dependent on four dimensions: θ, φ, λ and time. To calculate the seasonal mean with equivalent latitude, the isentropic PV fields, trace gas fields and the respective gradients are transformed into equivalent latitudes. The array size is reduced to two dimensions, θ and φ_e. Figures 4a and 4c show the seasonal mean isentropic O_3 gradient in φ_e-θ coordinates for June-July-August (JJA) and December-January–February (DJF) 2008.

[34] In DJF, ∇O_3 with equivalent latitude is enhanced in the vicinity of the maximum zonal mean wind speed on all isentropes. ∇O_3 is largest on the 320–330 K isentropes, which is below the core of the subtropical jet stream around 350 K. This feature reflects a strong polar jet stream during DJF 2008. On each isentrope the maximum of ∇O_3 is closely related to φ_e^{TP}. On isentropes below the core of the subtropical jet stream the ∇O_3 maximum is further related to the 2 PVU isoline, since there is a close distance between the 2 PVU isoline and the PV gradient-based tropopause. This relationship is not seen on higher isentropes above 350 K. The zonal mean wind speed is weaker in JJA than in DJF, but the relationship between PV^{TP} and ∇O_3 is still obvious in this season.

[35] The seasonal mean CO gradient in φ_e-θ coordinates is also maximum in the tropopause region close to the jet streams (Figures 4b and 4d), but the consistency overall between ∇CO with the wind field and PV^{TP} is not as good as for O_3. The agreement between maximum ∇CO and φ_e^{TP} in φ_e-θ coordinates is better during JJA than during DJF. ∇CO has its maximum at an equivalent latitude poleward of φ_e^{TP} at around $\varphi_e = 40°$N for all isentropes above 320 K.

[36] The relationship among the trace gas gradients, the PV gradient-based tropopause, and the 2 PVU isoline is further analyzed in Figure 5. Here, the distribution of the mean isentropic trace gas gradients on 330, 350, and 370 K are shown for DJF in relative equivalent latitudes $\Delta\varphi_e^{TP}$ (Figures 5a and 5c) and $\Delta\varphi_e^{2PVU}$ (Figures 5b and 5d). Maximum ∇O_3 conforms to the location of the PV gradient-based tropopause, $\Delta\varphi_e^{TP} = 0$. These maxima, on the other hand, do not agree with the 2 PVU isoline and they appear poleward of $\Delta\varphi_e^{2PVU} = 0$ when using the relative equivalent latitude with respect to 2 PVU. Maximum ∇CO is observed on an equivalent latitude range, $\Delta\varphi_e^{TP}$ = 0°N–20°N, in the LS.

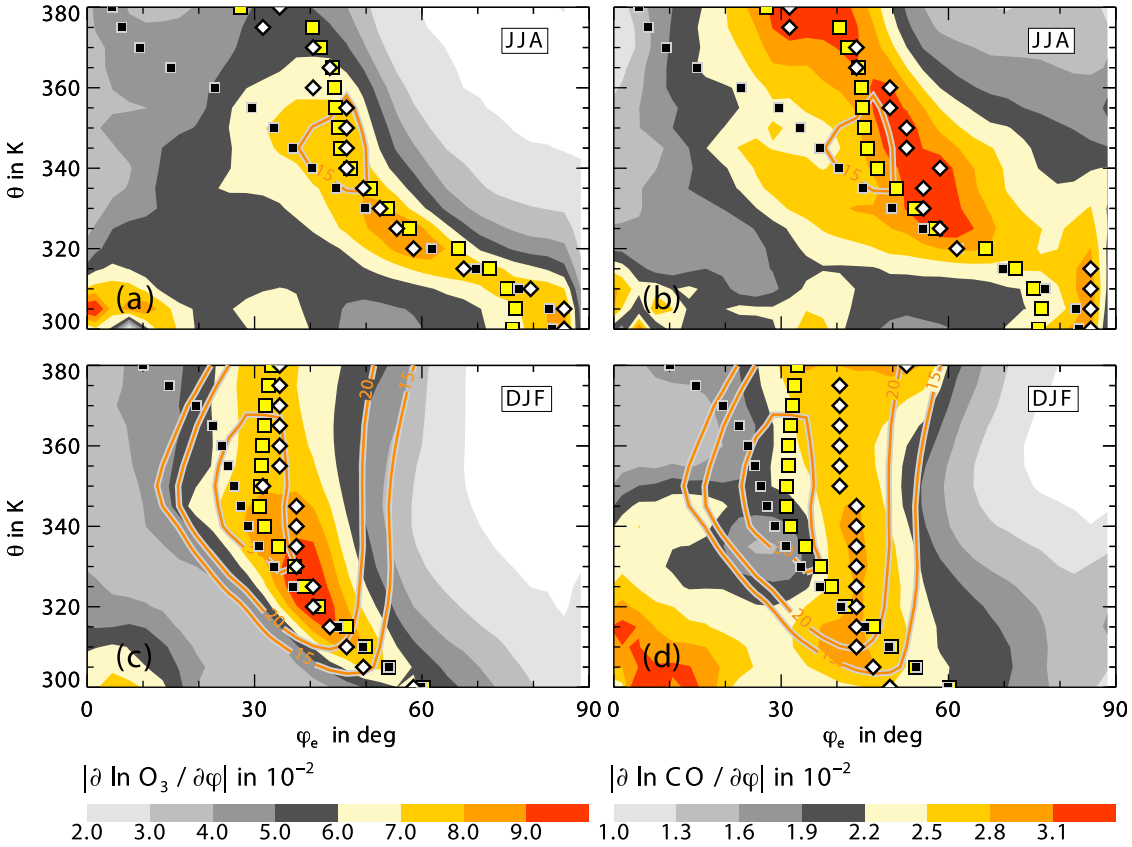

Figure 4. Seasonal mean WACCM isentropic gradient of (a and c) O_3 and (b and d) CO for summer (JJA) and winter (DJF) 2008 in $\theta - \varphi_e$ coordinates. PV^{TP} (yellow squares), 2 PVU isoline (black squares), and the maximum trace gas gradients (white diamonds) are indicated on each isentrope. Isolines of mean zonal wind speed are colored in orange.

[37] These results show that a better agreement between φ_e^{TP} and the gradients of the stratospheric and tropospheric tracers O_3 and CO is achieved by using φ_e-θ coordinates. The dynamical discontinuity is not colocated with the discontinuity in CO distribution consistently on all isentropes and for all seasons. Since the equivalent latitude represents the mean dynamics of the entire hemisphere, the local relationship between the dynamical and the chemical discontinuity dependent on geographical latitude and longitude is further examined.

4.3. Seasonal Mean Isentropic Gradients on 350 K

[38] Figure 6 shows the distribution of seasonal mean isentropic trace gas gradients in the Northern Hemisphere on 350 K for JJA and DJF 2008. Absolute values of isentropic gradients of O_3 and CO are calculated for each day in a season according to equation (3). The seasonal mean of ∇O_3 and ∇CO is calculated afterward.

[39] As shown in Figure 6, highest isentropic trace gas gradients, both of O_3 and CO, occur in the vicinity of PV^{TP} and the jet streams, both in JJA and DJF. Especially during DJF, when the jet stream is intense between 0°E and 180°E, a close relationship between the trace gas gradients, PV^{TP}, and the maximum wind speed is evident. The close relationship of the dynamical and chemical discontinuity indicates the presence of a strong transport barrier in this region, which is connected with an abrupt jump from tropospheric to stratospheric trace gas mixing ratios. The trace gas gradient is weaker in the western part of the Northern Hemisphere between the exit and entrance regions of the Pacific and Atlantic jet streams and the North American jet stream, respectively.

[40] Associated with frequent Rossby wave breaking (RWB) in these regions, the jet stream shows a characteristic split with a weakening of the horizontal wind speed. This region of wave breaking events is characterized by frequent mixing of trace gases from the stratosphere and troposphere [*Scott et al.*, 2001; *Waugh and Funatsu*, 2002]. Stratosphere-troposphere exchange across the tropopause may be preferred in these regions due to a weaker transport barrier. Consequently, these split jet stream regions are also characterized by split and weakened trace gas gradients in ∇O_3 and ∇CO. In this sense, the jet breaks also indicate a break of the tropopause on an isentropic surface.

[41] Nevertheless, the relationship between maximum ∇O_3 and PV^{TP} is closer than the relationship between ∇CO and PV^{TP} above North America extending to the western Atlantic. In this region maximum ∇CO is located poleward of PV^{TP} at 350 K as can be seen in Figure 4d. During JJA, isentropic trace gas gradients in the vicinity of the jet streams are in general weaker than during DJF. During JJA and DJF, the trace gas gradients in the western Northern Hemisphere are weaker compared with the eastern Northern Hemisphere. This may well be due to enhanced cross tropo-

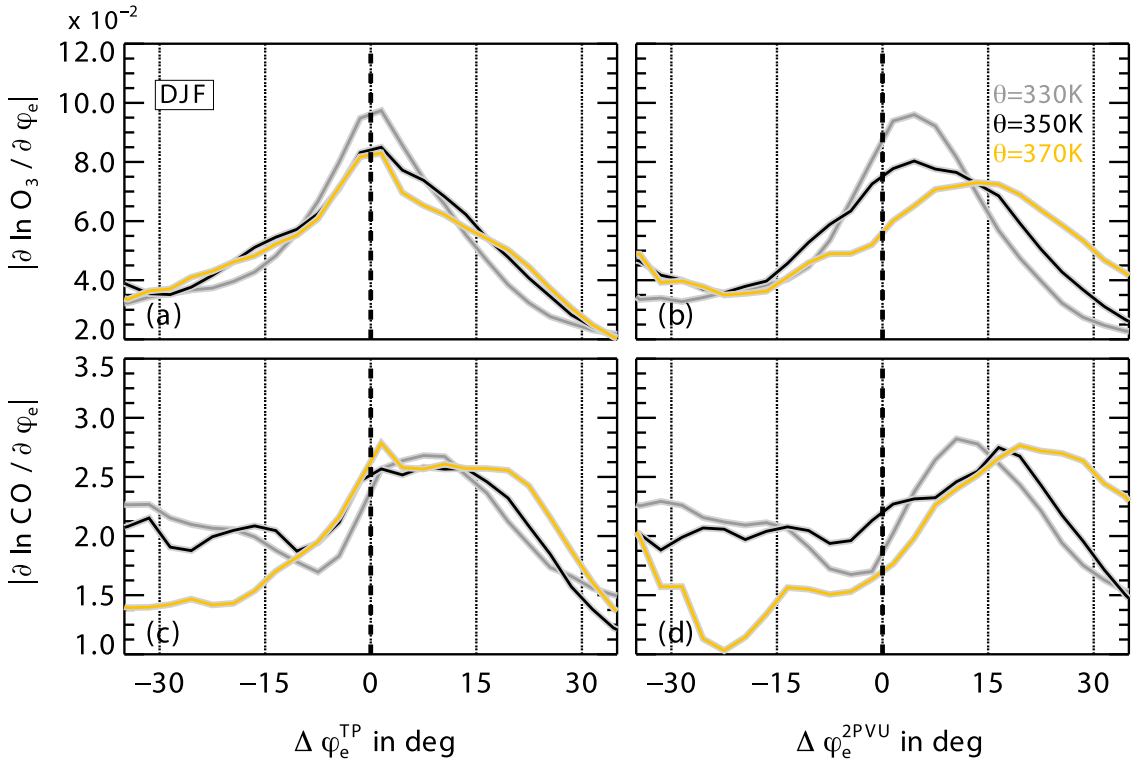

Figure 5. Seasonal mean WACCM profiles of absolute O_3 and CO gradients on three isentropes (330, 350, and 370 K) in DJF 2008. The gradients are shown in equivalent latitude distance relative to the (a and c) PV gradient–based tropopause $\Delta\varphi_e^{TP}$ and relative to the (b and d) 2 PVU isoline $\Delta\varphi_e^{2PVU}$.

pause exchange processes associated with the weakening of the jet stream in its split regions above the North Atlantic and Pacific.

[42] Although there is a slight discrepancy between ∇CO and PV^{TP} from North America toward the western Atlantic, a fairly good consistency is observed in other parts of the Northern Hemisphere between isentropic trace gas gradients, ∇O_3 and ∇CO, with PV^{TP} in the vicinity of jet streams. This indicates that in general the PV gradient-based definition well identifies the transport boundary at the tropopause. In addition, there are regions of anomalies where high trace gas gradients are decoupled from the dynamical tropopause. Anomalous high ∇O_3 is found southward of the downstream end of the North Pacific storm track region at around 15°N and 180°E in JJA which are located further westward at around 150°W in DJF. These anomalous high ∇O_3 are connected to a high O_3 mixing ratio and may in fact identify transport pathways of stratospheric air into the UT, since they are further consistent with regions of high frequency of stratospheric streamers and cutoffs on the same 350 K isentrope in both seasons [*Wernli and Sprenger*, 2007; *Sprenger et al.*, 2007]. In JJA ∇O_3 is weaker than in DJF. The shift of STE and high ∇O_3 from JJA to DJF in the zonal direction may be related to the strengthening of westerly ducts where mean westerly winds occur equatorward of the jet streams during winter. In particular, the enhanced zonal flow within the North Pacific westerly duct in DJF may favor the propagation of stratospheric streamers in the eastward direction which in turn may result in an eastward shift of high ∇O_3 from JJA to DJF.

[43] High ∇CO decoupled from the tropopause toward the equator are observed from eastern Africa to eastern Asia around 20°N and 30°E–150°E in JJA. These anomalous ∇CO maxima are also related to decoupled ∇O_3 between 120°E–150°E, whereas the related mixing ratios of CO (O_3) are higher (lower) than their background values in the UT. These trace gas gradients may be caused by deep convection processes above Asia and the western Pacific in JJA, which locally lead to rapid vertical transport of boundary layer air containing high CO pollution into the UTLS. This also provides an effective pathway for pollution from Asia, India, and Indonesia into the UT in JJA. In particular, the Asian monsoon deep convection transports CO and other pollution gases up to 12 km, near the level of main deep convective outflow at around 350 K [*Park et al.*, 2009; *Randel et al.*, 2010]. In the UTLS this high CO may be isentropically redistributed, e.g., boundary layer air with high CO content, that has been transported into the UT, may enter the midlatitude LS due to intrusion processes.

[44] Figure 7 shows an example of such a tropospheric intrusion from lower toward higher latitudes above the subtropical jet stream connected to a RWB event above the North Pacific recently described by *Homeyer et al.* [2011]. A streamer of tropospheric air with high CO penetrates toward the north at around λ = 180°E on 14 April 2008 and breaks up into the LS on 15 April 2008. PV^{TP}, represented by 6.1 PVU on 14 April 2008 and by 6.0 PVU on 15 April 2008, identifies this tropopause related process in contrast to the 2 or 4 PVU isolines. Both ∇CO and ∇O_3 are enhanced within this intrusion event.

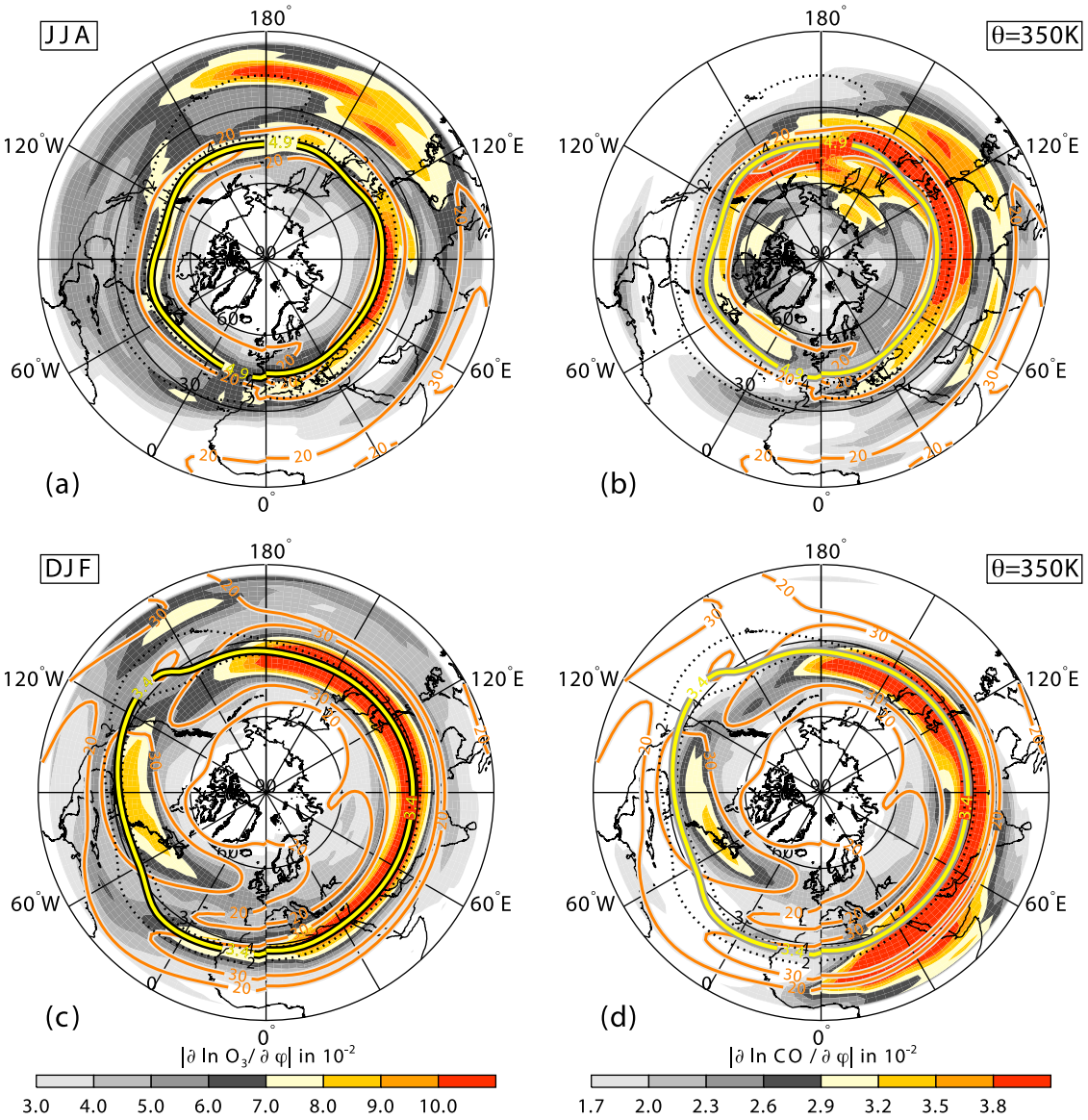

Figure 6. Seasonal mean WACCM gradient of (a and c) O_3 and (b and d) CO on the 350 K isentrope for DJF and JJA 2008. Mean PV^{TP} is represented by the 4.9 PVU isoline in JJA and by 3.4 PVU in DJF (yellow lines). The mean horizontal wind speed is highlighted by orange contours.

[45] These examples show that the analysis of isentropic gradients of trace gases, such as ∇O_3 and ∇CO, may help identifying the preferred transport pathways in the UTLS and the tropopause as a boundary between the UT and LS is identified by φ_e^{TP}. Nevertheless, there is a discrepancy between the location of maximum ∇CO and φ_e^{TP} above North America toward the western Atlantic during DJF (Figures 4 and 6), which is analyzed in section 4.4.

4.4. Sectional Mean Isentropic Gradients

[46] For a better understanding how trace gas gradients may be affected by local dynamics in specific regions, Figure 8 shows the mean isentropic distribution of ∇CO and ∇O_3 in $\varphi - \theta$ coordinates for DJF 2008 in two different Northern Hemisphere quadrants: Q1, $\lambda = 90°–180°$, central Asia and western Pacific; Q2, $\lambda = 270°–360°$, North Atlantic from the eastern United States to western Europe.

[47] These two different hemispheric quadrants, Q1 and Q2, were chosen for their different relationships between the dynamical and chemical discontinuity in the tropopause region (Figure 6). Q1 represents a region with a close relationship between the trace gas gradients, the jet streams and PV^{TP}, whereas Q2 is a region of split jet streams which is characterized by a weaker relationship between trace gas gradients and PV^{TP}.

[48] Figures 8a and 8b show the sectional zonal mean cross section of ∇O_3 and ∇CO from 300 to 380 K over the Q1 region for DJF 2008. ∇O_3 and ∇CO maxima are related to PV^{TP} in the vicinity of the jet stream over the Q1 region, which reflects the usefulness of the PV gradient-based tropopause to represent the chemical and the dynamical discontinuity. In contrast, there is a split jet stream over the Q2 region (Figures 8c and 8d). On isentropes above 340 K, a double jet stream structure, i.e., subtropical and polar jet

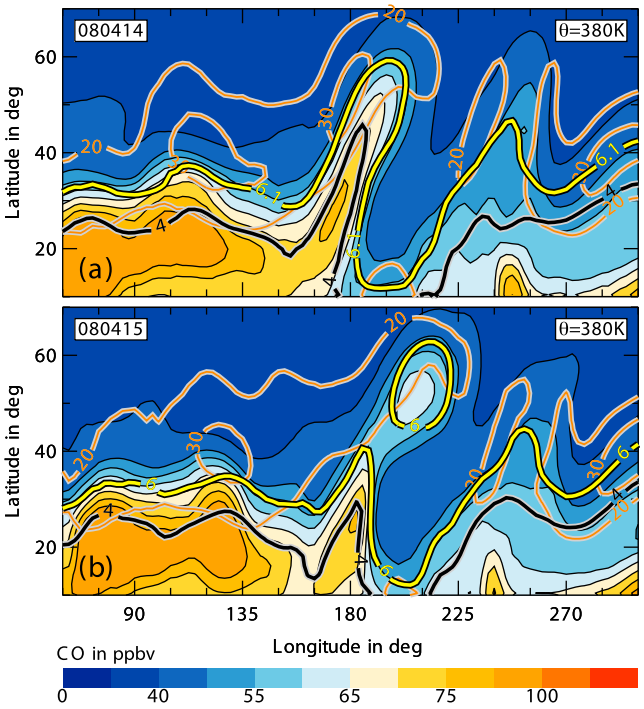

Figure 7. WACCM CO distribution at 380 K on (a) 14 April 2008 and (b) 15 April 2008. PV^{TP} is represented by the 6.1 PVU isoline on 14 April and by the 6.0 PVU isoline on 15 April 2008 (yellow line). The 4 PVU isoline (black line) and the horizontal wind speed (orange contours) are also shown.

stream, is present in this sectional mean, with the cores of the subtropical jet stream at 345 K at φ = 20°N and of the polar jet stream at 320 K at φ = 50°N. Maximum ∇O_3 are closely related to PV^{TP} and the jet streams in the seasonal mean. On lower isentropes both O_3 and PV^{TP} follow the polar jet stream, and on higher isentropes they follow the subtropical jet stream, respectively. This consistency is not observed for ∇CO. Maximum ∇CO represents the polar jet stream at around φ = 50°N on all isentropes above 320 K, but do not have a clear association with the subtropical jet stream structure at lower latitudes. This discrepancy in the Q2 region also accounts for the poleward offset of ∇CO in φ_e-θ coordinates in Figures 4 and 5.

[49] To further analyze this offset in trace gas gradient, Figures 9a–9d show the sectional zonal mean O_3 and CO distribution over the Q1 and Q2 regions in DJF 2008. There is a clear difference in the CO distribution in the vicinity of the subtropical jet stream between the Q1 and the Q2 region.

[50] PV^{TP} is associated with an intense jet stream and with a sharp transition of both trace gas distributions from the troposphere to the stratosphere over the Q1 region. Here, high CO from the boundary layer may be transported by convection above the landmasses into the UT in the tropics and subtropics (φ = 0°N–30°N), and may reach the tropical tropopause at around 380 K.

[51] In contrast, the dynamics over the Q2 region may influence the trace gas distribution in this region in a different manner than over the Q1 region. The Q2 region is characterized by a split jet stream. While a CO mixing ratio larger than 90 ppbv is observed up to 360 K at approximately φ = 20°N over the Q1 region, the same CO mixing

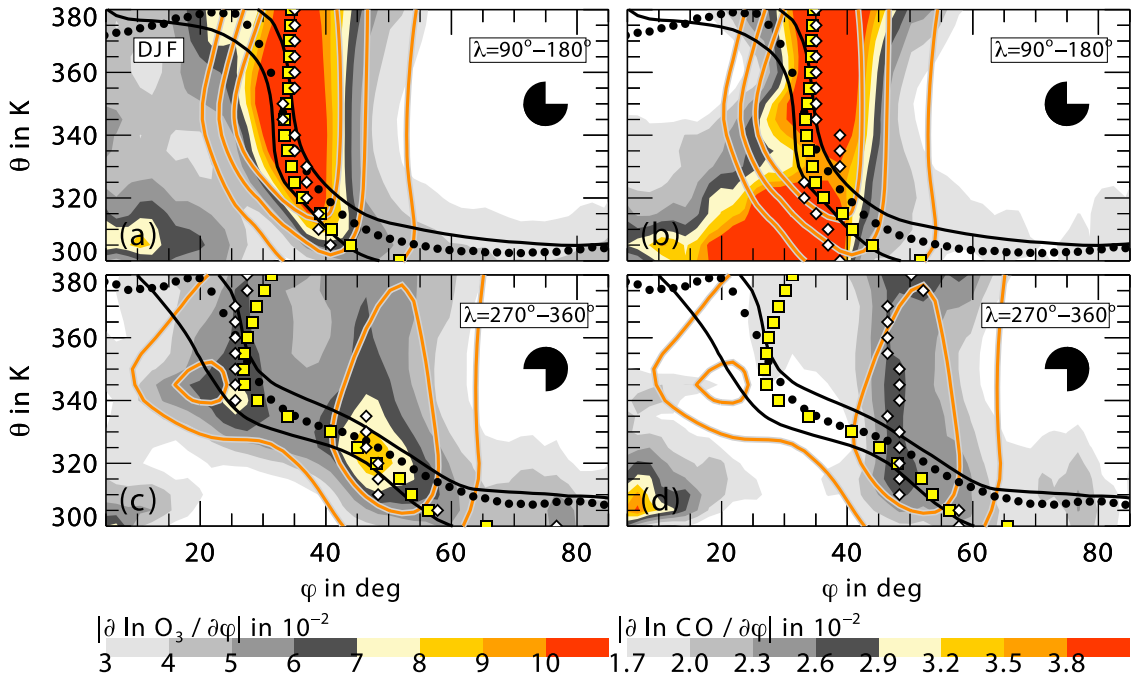

Figure 8. Zonal mean WACCM O_3 and CO gradient (a and b) above Asia (90°–180°) and (c and d) above the North Atlantic (270°–360°) on 300–380 K isentropes for DJF 2008. Mean PV^{TP} (yellow squares) and maximum trace gas gradients (white diamonds) are shown for each isentrope. Mean 2 and 4 PVU isolines (black contours), mean zonal wind speed (orange contours), and mean thermal tropopause (black dots) are highlighted.

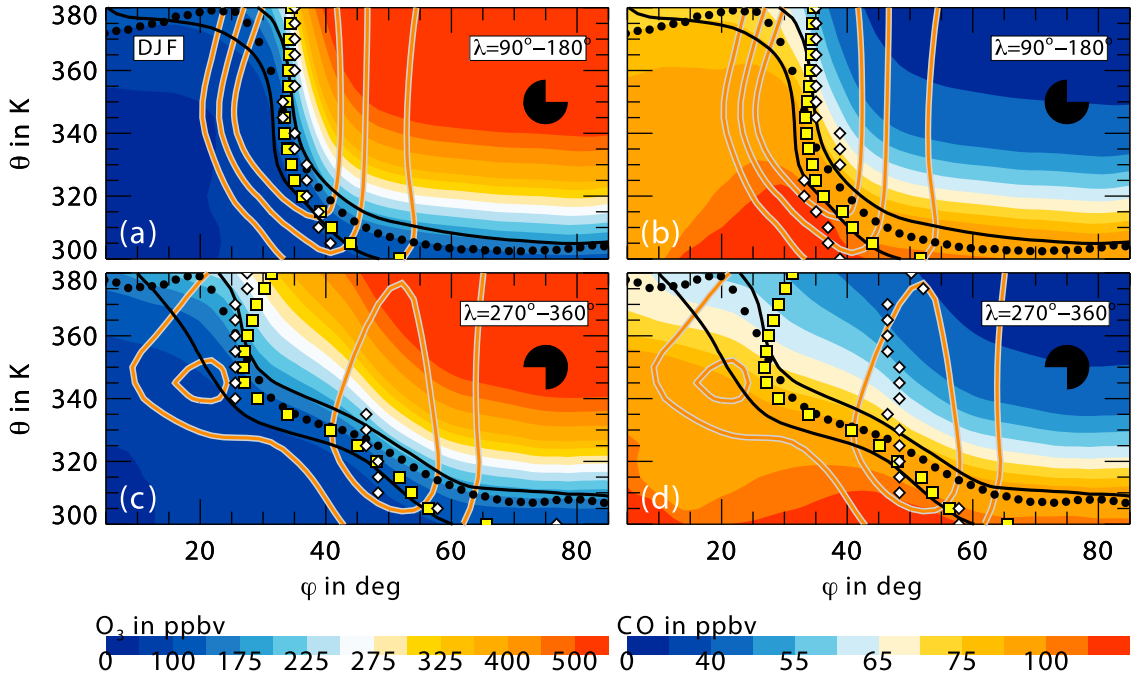

Figure 9. Same as Figure 8 but for mean isentropic O_3 and CO.

ratio occurs below the subtropical jet core at around 345 K over the Q2 region. This may be partly explained by the relatively weak convective activity above the North Atlantic at around φ = 20°N. The tropical tropopause layer (TTL), vertically extending from 350 to 420 K and horizontally bounded by the position of the subtropical jet stream [*Konopka et al.*, 2007; *Fueglistaler et al.*, 2009], seems to be horizontally less well bounded over the Q2 region than over the Q1 region. The region above the subtropical jet core at 345 K in the Q2 region is characterized by a strong cross-isentropic gradient of CO. The corresponding CO distribution is rather characterized by a stratospheric signal since the CO distribution is similar to that in the extratropical LS.

[52] There may likely be an enhanced isentropic exchange of air masses between the TTL at lower latitudes and the lowermost stratosphere (LMS) in the extratropics over the Q2 region compared with the Q1 region. A less strong barrier between the TTL and the LMS is also indicated by weaker trace gas gradients in O_3 and CO over the Q2 region compared with the Q1 region (see Figure 8). Isentropic exchange on high isentropes in particular regions of the Northern Hemisphere may therefore favor a disagreement between the location of the quasi-horizontal CO gradient, ∇CO, and PV^{TP}. The stratospheric tracer O_3 which is less influenced by tropospheric convection in the UTLS is also characterized by a similar trace gas distribution in the TTL and the lowermost stratosphere above the Q2 region.

[53] The results show that regions with a significant relationship between PV^{TP} and trace gas gradients identify the transport barrier on isentropes. In other regions where this relationship is weaker, the PV gradient-based tropopause may represent a more permeable boundary between the stratosphere and troposphere.

[54] The relation between PV^{TP} and the gradients of different trace gases characterized by different lifetimes is also examined (not shown). The tropospheric tracers HCFC-22 and N_2O are characterized by the same discrepancy between the chemical and dynamical discontinuity above the North Pacific as CO, while the stratospheric tracer HCl shows a similar agreement as observed for O_3. These results are also achieved for other years between 2004 and 2007.

[55] In the following, the seasonal behavior of the relation between the trace gas gradient and PV^{TP} is examined to further test the behavior of PV^{TP} as a boundary between the troposphere and stratosphere.

4.5. Annual Variation of Isentropic Trace Gradients

[56] The relationship between ∇O_3 and φ_e^{TP} is analyzed on different isentropes (330, 350, and 370 K). In contrast to CO, O_3 is less influenced by convection-driven processes in the troposphere and is better suited to test how well φ_e^{TP} identifies the boundary and transport barrier. Figures 10a–10c show the seasonal and annual variation of ∇O_3 in equivalent latitude on the three isentropes from 2004 to 2008. ∇O_3 is averaged with equivalent latitudes as described in section 4.2 for monthly bins.

[57] On each of the three isentropes, φ_e^{TP} identifies a strong transport barrier at the tropopause during winter (DJF) in each year. In general, ∇O_3 maxima are related to φ_e^{TP} in the vicinity of the jet stream in DJF. During summer (JJA), the transport barrier weakens and moves poleward [*Haynes and Shuckburgh*, 2000]. The tropopause appears to be more permeable, which is consistent with a weakening of ∇O_3 and the jet streams in Figure 10. PV^{TP} also identifies the poleward movement of the ∇O_3 in JJA.

[58] In addition, the 2 PVU isoline does not consistently identify the transport barrier on all isentropes. The discrepancy between 2 PVU and ∇O_3 maxima and the wind maxima increases from lower to higher isentropes. On the 370 K isentrope the 2 PVU isoline is totally decoupled from any dynamical and chemical discontinuity connected to the

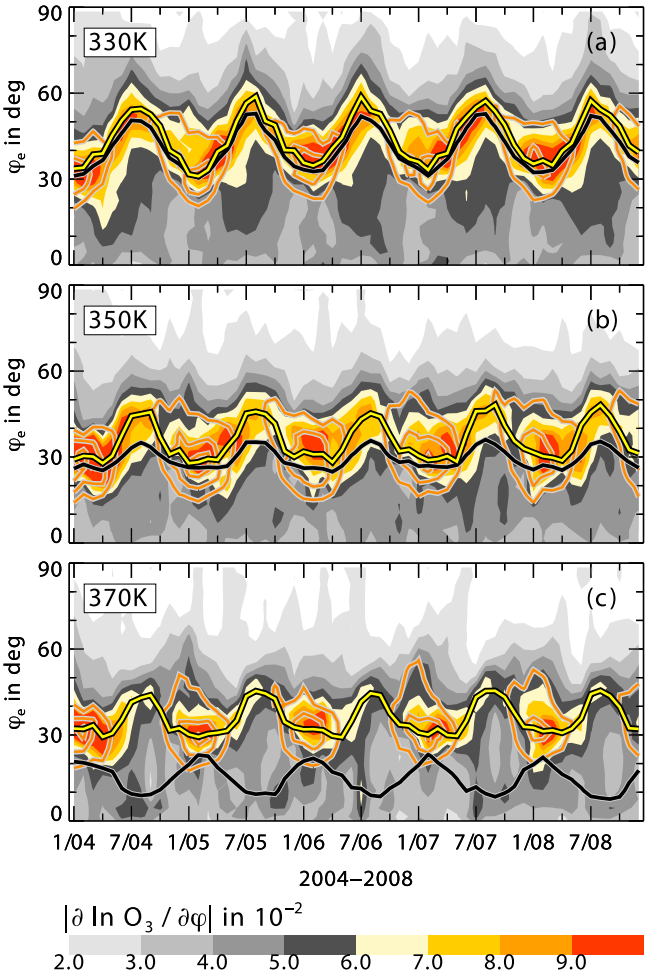

Figure 10. Temporal evolution of mean WACCM gradient of O_3 with equivalent latitude on three isentropes (330, 350, and 370 K) from 2004 to 2008. Mean PV^{TP} (yellow line), 2 PVU isoline (black line), and horizontal wind speed (orange contours) are plotted.

tropopause. It is even in an opposite phase with ∇O_3 and φ_e^{TP} as it moves equatorward during JJA.

[59] A well-established diagnostic of isentropic transport barriers is the eddy diffusivity based on potential vorticity [*Nakamura*, 1996; *Haynes and Shuckburgh*, 2000]. The seasonal evolution of ∇O_3 with equivalent latitude in the Northern Hemisphere, as shown in Figure 10, has a strong similarity with the eddy diffusivity diagnostic by *Haynes and Shuckburgh* [2000]. The stronger boundary during DJF is indicated by maximum ∇O_3 and a minimum eddy diffusivity reflecting a reduced mixing of trace gases across the tropopause. In JJA, the weakening of ∇O_3 is connected to an enhanced eddy diffusivity.

[60] *Berthet et al.* [2007] analyzed the location and seasonal evolution of the transport barrier associated with the tropopause based on trajectory calculations. They further defined a Lagrangian tropopause, which is marked by the proportion of trajectories visiting the boundary layer within a fixed time period. *Berthet et al.* [2007] found a difference between the position of the Lagrangian tropopause and the 2 PVU isoline, agreeing with our results on the discrepancy between the PV gradient-based tropopause and isentropic trace gas gradients with the 2 PVU isoline. The locations of the PV gradient-based tropopause and the Lagrangian tropopause reveal a pronounced seasonal cycle with a movement toward the pole in JJA and toward the equator in DJF on all isentropes. This seasonal cycle turns into an opposite phase from lower to higher isentropes when the tropopause is defined by the 2 PVU isoline (Figure 10).

[61] φ_e^{TP} is at 30°N during DJF when it is associated with a strong transport barrier from 330 to 370 K. In contrast, φ_e^{TP} moves further northward and becomes permeable during JJA. There is a seasonal cycle of the location of φ_e^{TP}, which spans a greater range of equivalent latitudes between JJA and DJF on lower than on higher isentropes (Figure 10). These results of the seasonal variation of φ_e^{TP} are in agreement with the variation of the Lagrangian tropopause of *Berthet et al.* [2007].

5. Discussion and Conclusions

[62] The chemical and dynamical discontinuity at the extratropical tropopause is analyzed using START08 and WACCM data. The study focuses on middle world isentropes between 300 and 380 K. This is a different approach complementary to studies investigating the vertical trace gas gradients using the altitude relative to the lapse rate tropopause [*Pan et al.*, 2004; *Hegglin et al.*, 2009; *Tilmes et al.*, 2010].

[63] The results support the PV gradient-based dynamical tropopause, PV^{TP}, as a diagnostic of the physical boundary in the UTLS [*Kunz et al.*, 2011]. The concept of PV^{TP} is examined with the help of isentropic gradients of O_3 and CO. The main results and the relevance and limitations of the approach are discussed in section 5.1.

5.1. Consistency of the Dynamical and Chemical Discontinuity

[64] The consistency overall between PV^{TP} and isentropic trace gas gradients of O_3 and CO, i.e., ∇O_3 and ∇CO, shows that PV^{TP} locates the isentropic chemical discontinuity well and therefore represents the transport boundary between the stratosphere and the troposphere. Maximum ∇O_3 and ∇CO are seen in the vicinity of the jet streams and follow the characteristic split above the North Atlantic and Pacific in DJF. Nevertheless, ∇O_3 is better related to PV^{TP} than ∇CO. This discrepancy may well be due to the fact that O_3 and CO have their dominant source regions in the stratosphere and troposphere, respectively.

[65] Dynamical processes in the troposphere, e.g., convective transport, which are different from those in the LS, e.g., adiabatic transport near the tropopause, may differently influence the UTLS distribution of tropospheric and stratospheric trace gases. The concept of PV^{TP} is largely a stratospheric concept, since it is based on equivalent latitude and PV as a passive and stratospheric tracer [*Danielsen and Hipskind*, 1980]. This may explain the sharp transition of the stratospheric tracer O_3 at PV^{TP}. In contrast, the sources of CO are in the boundary layer and convection transports CO into the UTLS. This makes the distribution of CO in the UTLS dependent on regional source regions and dynamics in the troposphere.

[66] ∇O_3 and ∇CO in the vicinity of the jet streams follow a seasonal cycle, with largest absolute values in DJF

and lowest absolute values and a poleward shift in JJA. PV^{TP}, as a boundary between the UT and LS, is connected to a strong transport barrier in DJF when high trace gas gradients are observed in its vicinity. In JJA, when the tropopause is known to be more permeable the related trace gas gradients are weakened. Nevertheless, in DJF regions of split jet streams are connected to mixing and STE [*Scott et al.*, 2001; *Waugh and Funatsu*, 2002] and these regions may consequently be characterized by low trace gas gradients and low PV gradients representing a permeable PV^{TP}.

[67] In the vicinity of jet streams, PV^{TP} follows ∇O_3 better than a fixed PV isoline. On isentropes above the core of the subtropical jet stream at around 350 K, a fixed PV isoline fails to represent the dynamical discontinuity and does not identify the boundary.

5.2. Trace Gas Gradients and Transport Pathways in the UTLS

[68] Regions with high ∇O_3 and ∇CO decoupled from the PV gradient-based tropopause and the jet streams are also shown. These anomalous gradients reveal the existence of preferred transport pathways in the UTLS. Two types of transport pathways are identified using trace gas gradients, which are discussed in the following.

[69] Enhanced ∇O_3 is observed above the North Pacific in DJF and above the eastern United States in JJA. A detailed analysis of ∇O_3 on synoptic and seasonal time scales with longitude at 350 K shows that high O_3 (low CO) is transported across the tropopause from the LS to the UT equatorward of the jet streams. On this isentrope STE processes are more frequent during JJA than during DJF [*Wernli and Sprenger*, 2007] and are related to ∇O_3 decoupled from the dynamical field equatorward of PV^{TP} above the North Pacific. A high frequency of streamers and cutoffs is also observed in the same region above the Pacific in DJF and the eastern United States in JJA [*Wernli and Sprenger*, 2007; *Sprenger et al.*, 2007].

[70] Enhanced ∇O_3 and ∇CO in the UTLS equatorward of PV^{TP} from Europe to Asia in JJA may be affected by convective processes. In JJA, convection transports high CO and low O_3 upward into the UTLS, e.g., the monsoon deep convection above Asia [*Park et al.*, 2009]. Anthropogenic boundary layer emissions may also be rapidly transported into the stratosphere by deep exchange processes with origins corresponding to the storm track entrance regions near the Asian or the North American East Coast [*Wernli and Bourqui*, 2002]. The regions of anomalous trace gas gradients in the UTLS are therefore associated with higher CO and lower O_3 contents compared to the unperturbed background atmosphere.

[71] This study has shown that STE processes can generally be identified by anomalous enhanced ∇O^3 and ∇CO which are decoupled from the dynamical field, i.e., PV^{TP}. A detailed analysis of these trace gas anomalies may therefore be valuable for understanding cross tropopause exchange processes. These enhanced trace gas gradients are further connected to specific values of PV^{TP}. The example of a RWB event at 380 K above the North Pacific can be identified by PV^{TP} = 6 PVU. This is consistent with the study of *Pan et al.* [2009], who observed stratospheric intrusions above the jet streams associated with the 6 PVU isoline.

5.3. Relevance and Limitation of the Approach

[72] Our analysis suggests that the PV gradient-based dynamical tropopause, PV^{TP}, is a general and fundamental concept to identify the boundary between the troposphere and stratosphere. This dynamical tropopause is consistent with the trace gas field and has the potential to identify and characterize STE processes.

[73] Nevertheless, PV^{TP} may have issues in representing the dynamical discontinuity on isentropes with two strong jet streams merging and meandering around the globe. The concept of PV^{TP} is based on a particular isoline of PV on an isentrope. Consequently, PV^{TP} can only represent a part of multiple jet streams meandering on a large regional extent, because the related isentropic wind field is not characterized by a pronounced maximum at a particular equivalent latitude. Since the determination of PV^{TP} is dependent on the horizontal wind speed and the PV gradient, PV^{TP} is described in these cases by the equivalent latitude connected to a maximum PV gradient. In multiple jet stream situations PV^{TP} may fail to accurately represent the dynamical discontinuity at all longitudes. The strength of the equivalent latitude approach of PV^{TP} is on the global distribution of the PV gradient and the horizontal wind field. The approach is limited, as it is missing some of these local features.

[74] Complex double jet streams should be rather analyzed by local analyses and may be better represented by a coordinate system relative to local maximum jet stream wind speeds [*Ray et al.*, 2004; *Manney et al.*, 2011]. *Manney et al.* [2011] recently performed a detailed analysis of the jet stream and plotted their data in relative latitude distances to the jet stream. For future work it would be interesting to examine how well each method works under complex jet structure conditions. This is reasonable, since the jet stream coordinate by *Manney et al.* [2011] may segregate air masses differently than our relative equivalent latitude coordinate, e.g., when analyzing features on the anticyclonic and cyclonic shear sides of the jet streams (L. L. Pan et al., Commentary on using equivalent latitude in the upper troposphere and lower stratosphere, submitted to *Atmospheric Chemistry and Physics*, 2011). In these cases, air masses with tropical equivalent latitude characteristics on the cyclonic side of the subtropical jet stream, e.g., tropospheric intrusions, may be connected with an equivalent latitude lower than that of the jet stream. Using the relative equivalent latitude coordinate, it is difficult to identify these intrusion events into the LS.

[75] Nevertheless, the equivalent latitude concept is well suited to identify the PV gradient-based tropopause, PV^{TP}, as a boundary in the UTLS. In multiple jet stream situations with a smooth wind field without any pronounced maximum in equivalent latitude coordinates, the maximum PV gradient, i.e., PV^{TP}, still represents the chemical discontinuity in ∇O_3. The jet streams therefore may not play the predominant role in determining the value of ∇O_3 as suggested by *Ray et al.* [2004]. In complex jet stream regions a comparison of PV^{TP} with the so-called e90 tropopause introduced by *Prather et al.* [2011] can be enlightening. Based on an artificial tracer e90 with surface sources and a 90 day decay time, *Prather et al.* [2011] mapped out the tropopause with a large seasonal variation of O_3. Since the e90 tropopause

captures complex features such as tropopause folds, it may also be worthwhile for the analysis of multiple jet stream situations.

[76] In the future, PV^{TP} may contribute to improved diagnostics of tropopause-related processes which otherwise may be biased due to ad hoc chosen values for the dynamical tropopause. Both for the identification of the transport barrier [*Haynes and Shuckburgh*, 2000; *Haynes et al.*, 2001], and for the quantification of cross tropopause mass exchange fluxes [*Wernli and Bourqui*, 2002; *Schoeberl*, 2004], the exact location of the tropopause is decisive.

[77] **Acknowledgments.** A. Kunz is supported by the German Academy of Sciences Leopoldina (LPDS 2009–25) and the visitor's program of the Atmospheric Chemistry Division at the National Center for Atmospheric Research (NCAR). NCAR is funded by the National Science Foundation. Fruitful discussions with Rolf Müller, Thomas Birner, and Tanya Peevey during the progress of this work are particularly acknowledged. Thanks to Heini Wernli and to two anonymous reviewers for their helpful comments.

References

Berthet, G., J. G. Esler, and P. H. Haynes (2007), A Lagrangian perspective of the tropopause and the ventilation of the lowermost stratosphere, *J. Geophys. Res.*, *112*, D18102, doi:10.1029/2006JD008295.

Butchart, N., and E. E. Remsberg (1986), The area of the stratospheric polar vortex for tracer transport on an isentopic surface, *J. Atmos. Sci.*, *43*, 1319–1339.

Cadle, R. D., R. Bleck, J. P. Shedlovsky, I. H. Blifford, J. Rosinski, and A. L. Lazrus (1969), Trace constituents in the vicinity of jet streams, *J. Appl. Meteorol.*, *8*, 348–356.

Danielsen, E. F. (1968), Stratospheric-tropospheric exchange based on radioactivity, ozone and potential vorticity, *J. Atmos. Sci.*, *25*, 502–518.

Danielsen, E. F., and R. S. Hipskind (1980), Stratospheric-tropospheric exchange at polar latitudes in summer, *J. Geophys. Res.*, *85*(C1), 393–400, doi:10.1029/JC085iC01p00393.

Danielsen, E. F., and V. A. Mohnen (1977), Project duststorm report: Ozone transport, in situ measurements, and meteorological analyses of tropopause folding, *J. Geophys. Res.*, *82*(37), 5867–5877, doi:10.1029/JC082i037p05867.

Emmons, L. K., et al. (2010), Description and evaluation of the Model for Ozone and Related chemical Tracers, version 4 (MOZART-4), *Geosci. Model Dev.*, *3*, 43–67, doi:10.5194/gmd-3-43-2010.

Folkins, I., P. Bernath, C. Boone, L. J. Donner, A. Eldering, G. Lesins, R. V. Martin, B.-M. Sinnhuber, and K. Walker (2006), Testing convective parameterizations with tropical measurements of HNO_3, CO, H_2O, and O_3: Implications for the water vapor budget, *J. Geophys. Res.*, *111*, D23304, doi:10.1029/2006JD007325.

Forster, P. M. de F., and K. P. Shine (1997), Radiative forcing and temperature trends from stratospheric ozone changes, *J. Geophys. Res.*, *102*(D9), 10,841–10,855, doi:10.1029/96JD03510.

Fueglistaler, S., A. E. Dessler, T. J. Dunkerton, I. Folkins, Q. Fu, and P. W. Mote (2009), Tropical tropopause layer, *Rev. Geophys.*, *47*, RG1004, doi:10.1029/2008RG000267.

Garcia, R. R., D. R. Marsh, D. E. Kinnison, B. A. Boville, and F. Sassi (2007), Simulation of secular trends in the middle atmosphere, 1950–2003, *J. Geophys. Res.*, *112*, D09301, doi:10.1029/2006JD007485.

Haynes, P., and E. Shuckburgh (2000), Effective diffusivity as a diagnostic of atmospheric transport: 2. Troposphere and lower stratosphere, *J. Geophys. Res.*, *105*(D18), 22,795–22,810, doi:10.1029/2000JD900092.

Haynes, P., J. Scinocca, and M. Greenslade (2001), Formation and maintenance of the extratropical tropopause by baroclinic eddies, *Geophys. Res. Lett.*, *28*(22), 4179–4182, doi:10.1029/2001GL013485.

Hegglin, M. I., C. D. Boone, G. L. Manney, and K. A. Walker (2009), A global view of the extratropical tropopause transition layer from Atmospheric Chemistry Experiment Fourier Transform Spectrometer O_3, H_2O, and CO, *J. Geophys. Res.*, *114*, D00B11, doi:10.1029/2008JD009984.

Hegglin, M. I., et al. (2010), Multimodel assessment of the upper troposphere and lower stratosphere: Extratropics, *J. Geophys. Res.*, *115*, D00M09, doi:10.1029/2010JD013884.

Held, I. M. (1982), On the height of the tropopause and the static stability of the troposphere, *J. Atmos. Sci.*, *39*, 412–417.

Hoerling, M. P., T. K. Schaack, and A. J. Lenzen (1991), Global objective tropopause analysis, *Mon. Weather Rev.*, *119*, 1816–1831.

Holton, J. R., P. H. Haynes, M. E. McIntyre, A. R. Douglass, R. B. Rood, and L. Pfister (1995), Stratosphere-troposphere exchange, *Rev. Geophys.*, *33*(4), 403–440, doi:10.1029/95RG02097.

Homeyer, C. R., K. P. Bowman, L. L. Pan, E. L. Atlas, R.-S. Gao, and T. L. Campos (2011), Dynamical and chemical characteristics of tropospheric intrusions observed during START08, *J. Geophys. Res.*, *116*, D06111, doi:10.1029/2010JD015098.

Hoskins, B. J., M. E. McIntyre, and A. W. Robertson (1985), On the use and significance of isentropic potential vorticity maps, *Q. J. R. Meteorol. Soc.*, *111*, 877–946.

Kinnison, D. E., et al. (2007), Sensitivity of chemical tracers to meteorological parameters in the MOZART-3 chemical transport model, *J. Geophys. Res.*, *112*, D20302, doi:10.1029/2006JD007879.

Konopka, P., et al. (2007), Contribution of mixing to upward transport across the tropical tropopause layer (TTL), *Atmos. Chem. Phys.*, *7*, 3285–3308.

Kunz, A., P. Konopka, R. Müller, and L. L. Pan (2011), Dynamical tropopause based on isentropic potential vorticity gradients, *J. Geophys. Res.*, *116*, D01110, doi:10.1029/2010JD014343.

Lamarque, J.-F., et al. (2011), CAM-chem: Description and evaluation of interactive atmospheric chemistry in CESM, *Geosci. Model Dev. Discuss.*, *4*, 2199–2278.

Logan, J. A. (1999), An analysis of ozonesonde data for the troposphere: Recommendations for testing 3-D models and development of a gridded climatology for tropospheric ozone, *J. Geophys. Res.*, *104*(D13), 16,115–16,149, doi:10.1029/1998JD100096.

Manney, G. L., et al. (2011), Jet characterization in the upper troposphere/lower stratosphere (UTLS): Applications to climatology and transport studies, *Atmos. Chem. Phys.*, *11*, 6115–6137.

Martius, O., C. Schwierz, and H. C. Davies (2010), Tropopause-level waveguides, *J. Atmos. Sci.*, *67*, 866–879, doi:10.1175/2009JAS2995.1.

Nakamura, N. (1996), Two-dimensional mixing, edge formation, and permeability diagnosed in an area coordinate, *J. Atmos. Sci.*, *53*, 1524–1537.

Nash, E. R., P. A. Newman, J. E. Rosenfield, and M. R. Schoeberl (1996), An objective determination of the polar vortex using Ertel's potential vorticity, *J. Geophys. Res.*, *101*(D5) 9471–9478, dio:10.1029/95JD00066.

Pan, L. L., W. J. Randel, B. L. Gary, M. J. Mahoney, and E. J. Hintsa (2004), Definition and sharpness of the extratropical tropopause: A trace gas perspective, *J. Geophys. Res.*, *109*, D23103, doi:10.1029/2004JD004982.

Pan, L. L., W. J. Randel, J. C. Gille, W. D. Hall, B. Nardi, S. Massie, V. Yudin, R. Khosravi, P. Konopka, and D. Tarasick (2009), Tropospheric intrusions associated with the secondary tropopause, *J. Geophys. Res.*, *114*, D10302, doi:10.1029/2008JD011374.

Pan, L. L., et al. (2010), The stratosphere-troposphere analyses of regional transport 2008 (START08) experiment, *Bull. Am. Meteorol. Soc.*, *91*, 327–342.

Park, M., W. J. Randel, L. K. Emmons, and N. J. Livesey (2009), Transport pathways of carbon monoxide in the Asian summer monsoon diagnosed from Model of Ozone and Related Tracers (MOZART), *J. Geophys. Res.*, *114*, D08303, doi:10.1029/2008JD010621.

Prather, M. J., X. Zhu, Q. Tang, J. Hsu, and J. L. Neu (2011), An atmospheric chemist in search of the tropopause, *J. Geophys. Res.*, *116*, D04306, doi:10.1029/2010JD014939.

Randel, W. J., M. Park, L. Emmons, D. Kinnison, P. Bernath, K. A. Walker, C. Boone, and H. Pumphrey (2010), Asian monsoon transport of pollution to the stratosphere, *Science*, *328*, 611–613, doi:10.1126/science.1182274.

Ray, E. A., K. H. Rosenlof, E. Richard, D. Parrish, and R. Jakoubek (2004), Distributions of ozone in the region of the subtropical jet: An analysis of in situ aircraft measurements, *J. Geophys. Res.*, *109*, D08106, doi:10.1029/2003JD004143.

Reed, R. J. (1955), A study of a characteristic type of upper-level frontogenesis, *J. Meteorol.*, *12*, 226–237.

Schoeberl, M. R. (2004), Extratropical stratosphere-troposphere mass exchange, *J. Geophys. Res.*, *109*, D13303, doi:10.1029/2004JD004525.

Schwierz, C., S. Dirren, and H. C. Davies (2004), Forced waves on a zonally aligned jet stream, *J. Atmos. Sci.*, *61*, 73–87.

Scott, R. K., J.-P. Cammas, P. Mascart, and C. Stolle (2001), Stratospheric filamentation into the upper tropical troposphere, *J. Geophys. Res.*, *106*, 11,835–11,848, doi:10.1029/2001JD900049.

Shapiro, M. A. (1980), Turbulent mixing within tropopause folds as a mechanism for exchange of chemical constituents between the stratosphere and troposphere, *J. Atmos. Sci.*, *37*, 994–1004.

Shapiro, M. A., T. Hampel, and A. J. Krueger (1987), The Arctic tropopause fold, *Mon. Weather Rev.*, *115*, 444–454.

Simmons, A., M. Hortal, G. Kelly, A. McNally, A. Untch, and S. Uppala (2005), ECMWF analyses and forecasts of stratospheric winter polar vortex breakup: September 2002 in the Southern Hemisphere and related events, *J. Atmos. Sci.*, *62*, 668–689.

Solomon, S., K. H. Rosenlof, R. W. Portmann, J. S. Daniel, S. M. Davis, T. J. Sanford, and G.-K. Plattner (2010), Contributions of stratospheric water vapor to decadal changes in the rate of global warming, *Science*, *327*, 1219–1223.

Sprenger, M., H. Wernli, and M. Bourqui (2007), Stratosphere-troposphere exchange and its relation to potential vorticity streamers and cutoffs near the extratropical tropopause, *J. Atmos. Sci.*, *64*, 1587–1602.

Stohl, A., H. Wernli, P. James, M. Bourqui, C. Forster, M. A. Liniger, P. Seibert, and M. Sprenger (2003), A new perspective of stratosphere-troposphere exchange, *Bull. Am. Meteorol. Soc.*, *84*, 1565–1573, doi:10.1175/BAMS-84-11-1565.

Tilmes, S., et al. (2010), An aircraft-based upper troposphere lower stratosphere O_3, CO, and H_2O climatology for the Northern Hemisphere, *J. Geophys. Res.*, *115*, D14303, doi:10.1029/2009JD012731.

Vogel, B., et al. (2011), Transport pathways and signatures of mixing in the extratropical tropopause region derived from Lagrangian model simulations, *J. Geophys. Res.*, *116*, D05306, doi:10.1029/2010JD014876.

Waugh, D. W., and B. M. Funatsu (2002), Intrusions into the tropical upper troposphere: Three-dimensional structure and accompanying ozone and OLR distributions, *J. Atmos. Sci.*, *60*, 637–653.

Wernli, H., and M. Bourqui (2002), A Lagrangian "1-year climatology" of (deep) cross-tropopause exchange in the extratropical Northern Hemisphere, *J. Geophys. Res.*, *107*(D2), 4021, doi:10.1029/2001JD000812.

Wernli, H., and M. Sprenger (2007), Identification and ERA-15 climatology of potential vorticity streamers and cutoffs near the extratropical tropopause, *J. Atmos. Sci.*, *64*, 1569–1586.

World Meteorological Organization (1957), Meteorology: A three-dimensional science, *WMO Bull. 6*, 134–138, Geneva, Switzerland.

World Meteorological Organization (1986), Scientific assessment of atmospheric ozone, *Rep. 16*, WMO Global Ozone Res. and Mon. Proj., Geneva, Switzerland.

D. E. Kinnison, L. L. Pan, and S. Tilmes, National Center for Atmospheric Research, PO Box 3000, Boulder, CO 80307, USA.

P. Konopka and A. Kunz, Institut für Energie- und Klimaforschung: Stratosphäre, Forschungszentrum Jülich, Wilhem-Jonen Strasse, D-52425 Jülich, Germany. (a.kunz@fz-juelich.de)